JCI insight

RESEARCH ARTICLE

Heat-killed *Mycobacterium tuberculosis* prime-boost vaccination induces myeloid-derived suppressor cells with spleen dendritic cell–killing capability

Eliana Ribechini,[1] Ina Eckert,[1] Andreas Beilhack,[2] Nelita Du Plessis,[3] Gerhard Walzl,[3] Ulrike Schleicher,[4] Uwe Ritter,[5] and Manfred B. Lutz[1]

[1]Institute of Virology and Immunobiology, University of Würzburg, Würzburg, Germany. [2]Department of Internal Medicine II, University Hospital Würzburg, Würzburg, Germany. [3]South African Medical Research Council, Centre for Tuberculosis Research, Department of Science and Technology – National Research Foundation Centre of Excellence for Biomedical Tuberculosis Research, Division of Molecular Biology and Human Genetics, Faculty of Medicine and Health Sciences, Stellenbosch University, Cape Town, South Africa. [4]Microbiology Institute, Clinical Microbiology, Immunology and Hygiene, Universitätsklinikum Erlangen, Friedrich-Alexander-Universität Erlangen-Nürnberg, Erlangen, Germany. [5]RCI Regensburg Center for Interventional Immunology, Institute of Immunology, University Medical Center Regensburg, University of Regensburg, Regensburg, Germany.

Tuberculosis patients and mice infected with live *Mycobacterium tuberculosis* accumulate high numbers of myeloid-derived suppressor cells (MDSCs). Here, we hypothesized that dead *M. tuberculosis* vaccines also may induce MDSCs that could impair the efficacy of vaccination. We found that repeated injections of *M. tuberculosis* vaccines (heat-killed *M. tuberculosis* in incomplete Freund's adjuvant, such as Montanide) but not single or control vaccines without *M. tuberculosis* strongly expanded CD11b$^+$ myeloid cells in the spleen, leading to T cell suppression of proliferation and killing ex vivo. Dead *M. tuberculosis* vaccination induced the generation of CD11b$^+$Ly6C^{hi}CD115$^+$ iNOS/*Nos2*$^+$ monocytic MDSCs (M-MDSCs) upon application of inflammatory or microbial activation signals. In vivo these M-MDSCs were positioned strategically in the splenic bridging channels and then positioned in the white pulp areas. Notably, within 6–24 hours, in a *Nos2*-dependent fashion, they produced NO to rapidly kill conventional and plasmacytoid DCs while, surprisingly, sparing T cells in vivo. Thus, we demonstrate that *M. tuberculosis* vaccine induced M-MDSCs do not directly suppress effector T cells in vivo but, instead, indirectly by killing DCs. Collectively, we demonstrate that *M. tuberculosis* booster vaccines induce M-MDSCs in the spleen that can be activated to kill DCs. Our data suggest that formation of MDSCs by *M. tuberculosis* vaccines should be investigated also in clinical trials.

Conflict of interest: The authors have declared that no conflict of interest exists.

Submitted: March 6, 2019
Accepted: May 24, 2019
Published: July 11, 2019.

Reference information: *JCI Insight*. 2019;4(13):e128664. https://doi.org/10.1172/jci.insight.128664.

Introduction

Myeloid-derived suppressor cells (MDSCs) negatively regulate cell-mediated immunity by inhibiting T cell proliferation and inducing Treg responses (1). Although widely characterized by their expression of Gr-1 and CD11b markers, MDSCs can be further subdivided into monocytic CD11b$^+$Ly6G$^-$Ly6C^{hi} MDSCs and granulocytic CD11b$^+$Ly6G$^+$Ly6C^{lo} MDSC subsets in mice (1). Among many different suppressor mechanisms of MDSCs (2), the production of NO by the activity of the inducible NO synthase (iNOS) appears to be a suppressive tool mainly described for the monocytic MDSC (M-MDSC) subset (3). However, to date, NO production and its direct role in T cell suppression have been shown only in cocultures of T cells stimulated for proliferation with MDSCs in vitro and ex vivo (4–7). The demonstration of direct NO-dependent T cell suppression by MDSCs in vivo is lacking.

Suppressive effects of MDSCs have been mainly observed in tumor biology, but there is increasing evidence of similar effects in infectious disease conditions, especially for the M-MDSC subset in tuberculosis (TB) (8). Previously, we observed that MDSCs are highly induced in patients suffering from TB and in children coinfected with HIV (9, 10). MDSC accumulation was also proved to be a critical regulator in murine

models of live *Mycobacterium tuberculosis* infection (11). Whether vaccines containing killed *M. tuberculosis* would also induce MDSCs remains unclear.

Among the carrier substances for antitumor or antipathogen vaccines, incomplete Freund's adjuvant (IFA), used under the name Montanide ISA-51 VG, is a suitable and widely distributed mineral oil–based adjuvant for human clinical studies with good antigen responses but also some adverse effects (12, 13). Another preparation, CFA, was developed in 1942 and since then has been widely used as a vaccine adjuvant in experimental animals (14). Since CFA is composed of IFA containing heat-killed and dried *M. tuberculosis*, it can be considered as an *M. tuberculosis* vaccine. Notably, unclear tolerogenic effects had been observed after CFA vaccination in animals (14). On the one hand, CFA is a critical component for the induction of autoimmunity in models of experimental autoimmune encephalomyelitis (15, 16); on the other hand, injection of CFA could also prevent autoimmunity, such as the onset of type I diabetes in NOD mice (17) and ameliorated Parkinson's disease in rats (18). While the pathogen-induced adjuvant effects can be explained by mycobacterial triggering of TLR2 and TLR4, the tolerogenic mechanisms of CFA are not understood. The possible suppressive effects, besides their immunostimulatory function by IFA and other adjuvants in tumor vaccination studies, have been reviewed before (13). CFA-based tumor vaccines could induce suppressive $CD11b^+$ immune cells (7, 19), while in an alum-based vaccine, B cell immune responses were boostered by $CD11b^+$ cells (19). However, these questions remain unclear: whether *M. tuberculosis* or IFA/Montanide will be able to induce MDSCs, which MDSC subsets will become activated, and what are the major target cells of their suppression in vivo.

Previously, we described a simple and reliable protocol to generate murine MDSCs in vitro from murine BM precursor cells with GM-CSF (20). The generation of such human or murine M-MDSCs in vitro can be performed by following a 2-step protocol that, first, converts classical monocytes ($Ly6C^{hi}$ or $CD14^+$) into monocytes "licensed" for suppression (L-Mono) that also can be considered as resting M-MDSCs and, second, converts L-Mono into activated M-MDSCs that release the suppressor molecules NO in the murine and IDO in the human system (21). This in vitro differentiation model exemplifies the 2 steps of signaling for M-MDSC induction that are relevant also in vivo (1). While the combination of LPS and IFN-γ for the second step of MDSC activation constituted one of the strongest signals (22), cocktails of proinflammatory cytokines were also effective (21). While the infiltration of MDSCs at vaccination sites and lymph nodes has been observed before using *Mycobacterium bovis* BCG, only local T cell responses seemed to be affected in these organs (23).

The targets of MDSC-mediated suppression were mainly identified as macrophages, NK cells, and $CD4^+$ or $CD8^+$ T cells that were tested for their phagocytic activity, proliferative capacity, or their production of cytokines (2, 24). DCs, which represent key mediators to induce adaptive immune responses, can be affected by MDSCs in tumors, mostly by converting them into tolerogenic phenotypes (25). Other regulatory myeloid cells, such as regulatory macrophages, have been shown to impair DC maturation indirectly by inducing Tregs (26). However, whether MDSCs effect DC function during infection or vaccination has not been addressed yet. Here, we show that MDSCs induce apoptosis of BM-generated DCs (BM-DCs) in vitro and conventional DCs (cDCs) and plasmacytoid DCs (pDCs) in the T cell areas of the splenic white pulp of mice. DC killing depended on iNOS and the release of NO. Our data demonstrate that a *M. tuberculosis* vaccine, such as a component of CFA, induces licensing and activation of MDSCs in mice. These CFA-induced MDSCs readily produced NO and were primarily found to induce apoptosis in DC subsets rather than T cells.

These results suggest a potentially new immune evasion mechanism of DC killing by *M. tuberculosis* that does not rely on live bacteria but occurs after killed *M. tuberculosis* vaccination. Given the pivotal role of DCs for vaccine success, and new TB control strategies by applying revaccination, these potentially novel findings may significantly effect the future design and monitoring of *M. tuberculosis* vaccination strategies.

Results

CFA expands the myeloid cell compartment in the splenic red pulp. To examine how *M. tuberculosis* vaccines influence the composition of the myeloid compartment and MDSC generation and activation, most of the following experiments were performed according to defined protocols of immunization. These include application of CFA alone or followed by a second IFA or CFA injection. Optionally, short-term challenges by LPS/IFN-γ injections were performed before spleens were analyzed (Figure 1A). When we injected mice s.c. with a single CFA dose splenic cell numbers increased, similar to that in previous reports (7, 27), and a double immunization by the CFA/CFA regimen further increased the number of splenic myeloid

cells (Figure 1B). The frequency of granulocytic Ly6C$^+$Ly6G$^+$ cells was boosted especially after the first and second CFA application, and the frequencies of Ly6C^{hi} monocytic cells were moderately increased (Figure 1C). To address the spatial localization of the endogenous, CFA-expanded cells within the spleen, we stained sections from cryopreserved spleens from healthy, CFA-, and CFA/CFA-injected mice for different markers. All Gr-1$^+$ cells were restricted to the splenic red pulp area independent of their expansion by CFA or CFA/CFA immunizations (Figure 1D). To gain a more detailed insight on the phenotype of CFA-expanded cells, we employed markers frequently used for the identification of MDSCs for immunofluorescence staining of spleens from CFA-treated mice. CD11b$^+$ cells coexpressed Gr-1, Ly6C, and Ly6G markers but very little F4/80 (Supplemental Figure 1; supplemental material available online with this article; https://doi.org/10.1172/jci.insight.128664DS1), a finding compatible with the hypothesis that the CFA-expanded cells represent neutrophilic and monocytic cells rather than resident red pulp macrophages of embryonic origin (28). All together, these data suggest that CFA or CFA/CFA administration triggered the expansion and accumulation of myeloid spleen cells that phenotypically resemble both monocytic Ly6C^{hi}Ly6G$^-$ and granulocytic Ly6C^{lo}Ly6G$^+$ MDSC subsets.

Splenic CD11b$^+$ cells of CFA/CFA-immunized mice acquire NO-dependent T cells suppressor capacity. Next, we asked whether the expansion of splenic myeloid cells after the different CFA immunizations induced suppressor functions. For this purpose, we immunized mice either once with CFA or twice with the combinations CFA/IFA or CFA/CFA. Three days later, CD11b$^+$ cells from the spleens of these mice were purified as a source of myeloid cells containing the potential MDSC subsets. Their ability to produce NO was tested by an overnight treatment with LPS/IFN-γ, a method that had been established before ex vivo for splenic MDSCs (22) and as shown here in vitro (Supplemental Figure 2). Only splenic CD11b$^+$ cells derived from mice immunized with the CFA/CFA protocol produced amounts of NO that reached the levels of in vitro BM-generated MDSCs (Figure 2A).

To test whether this correlated with the acquisition of T cell suppressor potential, splenic CD11b$^+$ cells from the same groups of immunized mice were cultured with CD3/CD28 antibody-stimulated naive T cells. Detection of T cell proliferation by CFSE dilution indicated that only CD11b$^+$ cells from CFA/CFA mice acquired T cell suppressor potential on CD4$^+$ and CD8$^+$ T cells to the same levels as observed with BM-MDSCs (Figure 2, B and C). T cell suppression by CD11b$^+$ cells from CFA/CFA mice depended on NO release, because addition of the iNOS-inhibitor L-NMMA restored T cell proliferation (Figure 2, B and C). Thus, ex vivo–isolated splenic CD11b$^+$ cells from CFA/CFA-immunized mice but not mice immunized with CFA or the CFA/IFA combination underwent a monocyte-licensing process, which allowed the acquisition of MDSC suppressor potential on stimulated T cells from unperturbed mice.

To further test whether the T cells within the spleens that contain CD11b$^+$ suppressor cells appear as suppressed T cells, we labeled spleen cells obtained from control mice or CFA-, CFA/IFA-, and CFA/CFA-immunized mice with CFSE and stimulated them with CD3/CD28 antibodies for 4 days. CFA/CFA immunization significantly impaired the proliferation capacity of endogenous CD4$^+$ and CD8$^+$ T cells (Figure 2D). When the same experiment was performed, but splenic CD11b$^+$ cells were removed by magnetic beads before culture, the T cell proliferation of CFA/CFA-immunized mice was not affected (Figure 2E). These data clearly indicate that in spleens of CFA/CFA mice suppressive CD11b$^+$iNOS$^+$ cells are generated that control the proliferation capacity of naive or endogenous T cells by NO production ex vivo.

Since NO production for suppressor function of CD11b$^+$ cells is most likely derived from monocytic cells (Supplemental Figure 1, A and B), and splenic monocytes reside in the red pulp and subcapsular sinus (29) but are not localized within the T cell areas of the white pulp, the question remained of which anatomical location suppressor cells produce NO and suppress T cells in vivo.

LPS/IFN-γ challenge accumulates CD11b$^+$CD115$^+$iNOS$^+$ M-MDSCs in splenic T cell areas adjacent to DCs. Since ex vivo–isolated splenic CD11b$^+$ cells acquired iNOS-dependent T cell suppressor function, we attempted to detect iNOS in spleens of mice immunized with CFA or CFA/CFA. Immunofluorescence staining of cryopreserved spleens 3 days after the last CFA injection did not reveal any iNOS$^+$ cells in all groups of immunized mice (Figure 3A). Since the optimal time point for iNOS detection in the spleen after s.c. CFA immunization may be difficult to determine, we injected CFA/CFA-immunized mice peritoneally with the established LPS/IFN-γ regimen to induce iNOS. After 6 hours, this treatment induced massive infiltrations of CD11b$^+$ cell but moderate Ly6G$^+$ cell accumulation in the CD3$^+$ T cell areas of the white pulp in both WT and *Nos2*$^{-/-}$ mice (Figure 3B). The infiltrates also appeared as iNOS$^+$ cells in sections of WT mice but not of *Nos2*$^{-/-}$ mice (Figure 4A), confirming the specificity of our iNOS detection. Next, we asked whether the iNOS detection would indeed lead to the release of NO and whether

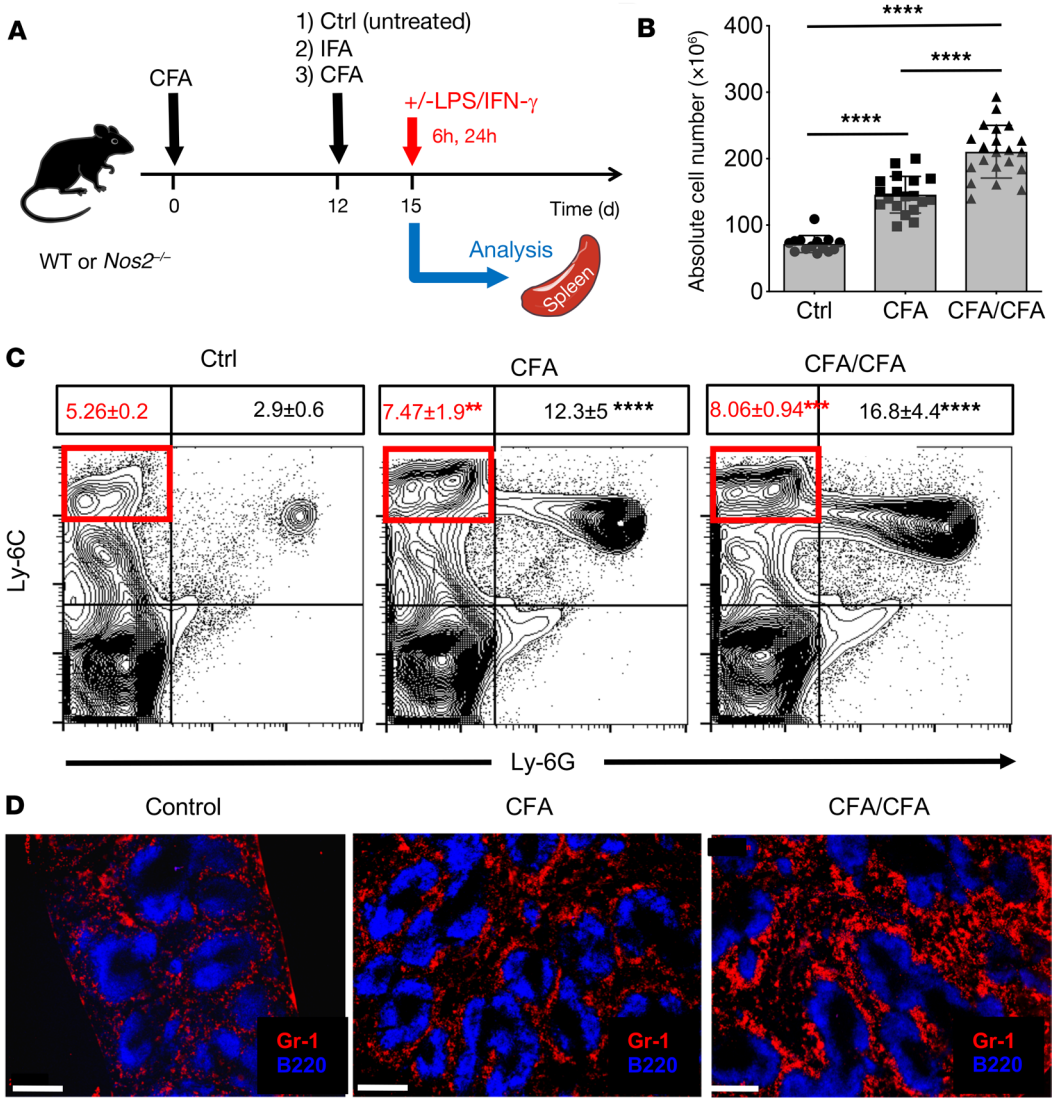

Figure 1. CFA administration induces myeloid cell expansion and accumulation in the splenic red pulp. (**A**) General scheme of single and repetitive immunizations. Mice received a single s.c. dose of CFA at day 0 alone or second dose of IFA or CFA at day 12. Then spleens were analyzed at day 15. Optionally, mice were challenged with LPS/IFN-γ at day 15 for 6 hours or 24 hours before spleens were further analyzed. (**B**) C57BL/6 mice were injected s.c. with CFA or CFA/CFA or remained untreated before spleens were analyzed according the scheme in **A**. Spleen cellularity was counted at day 15 (9 independent experiments with replicates: Ctrl = 14, CFA = 19, CFA/CFA = 21). (**C**) Mice were injected as described above, and spleen cells were analyzed by FACS for Ly6C$^+$ and Ly6G$^+$ cell subsets. Numbers above the dot plots represent the percentages of the red gated Ly6C^{hi} gated cells or the top right quadrant for Ly6G$^+$ cells (4 independent experiments with replicates: Ctrl = 9, CFA = 14, CFA/CFA = 11). (**D**) Spleens from the indicated mice were collected at day 15 and cryosections were stained for Gr-1 for myeloid cells and B220 to indicate B cell zones as borders of the white pulp. Scale bars: 500 μm. Microscopy data are representative of at least 3 independent experiments with (n = 3 mice) for each group. (**B** and **C**) Statistical significance was assessed by comparison of control versus treated mice. Statistics by 1-way ANOVA with multiple comparisons and Tukey's post test. $^{**}P < 0.01$, $^{***}P < 0.005$, $^{****}P < 0.0001$. Values correspond to the mean ± SD.

the LPS/IFN-γ challenge alone was responsible for NO induction but required preimmunization of the mice with CFA/CFA. Therefore, we challenged untreated control mice and mice treated with CFA only or CFA/CFA systemically with LPS/IFN-γ. After 6 hours, the NO production by DAQ staining of splenic cryosections was highly increased in the T cell areas of CFA/CFA-immunized mice, while it was only moderately detectable in spleens of mice injected with LPS/IFN-γ only or CFA plus LPS/IFN-γ–treated mice (Figure 4B). Together, despite the fact that spleens of CFA/CFA-injected mice contain functionally suppressive MDSCs with NO-producing capacity (Figure 2), iNOS was not detectable in the spleens of these mice but required LPS/IFN-γ challenge to be visualized.

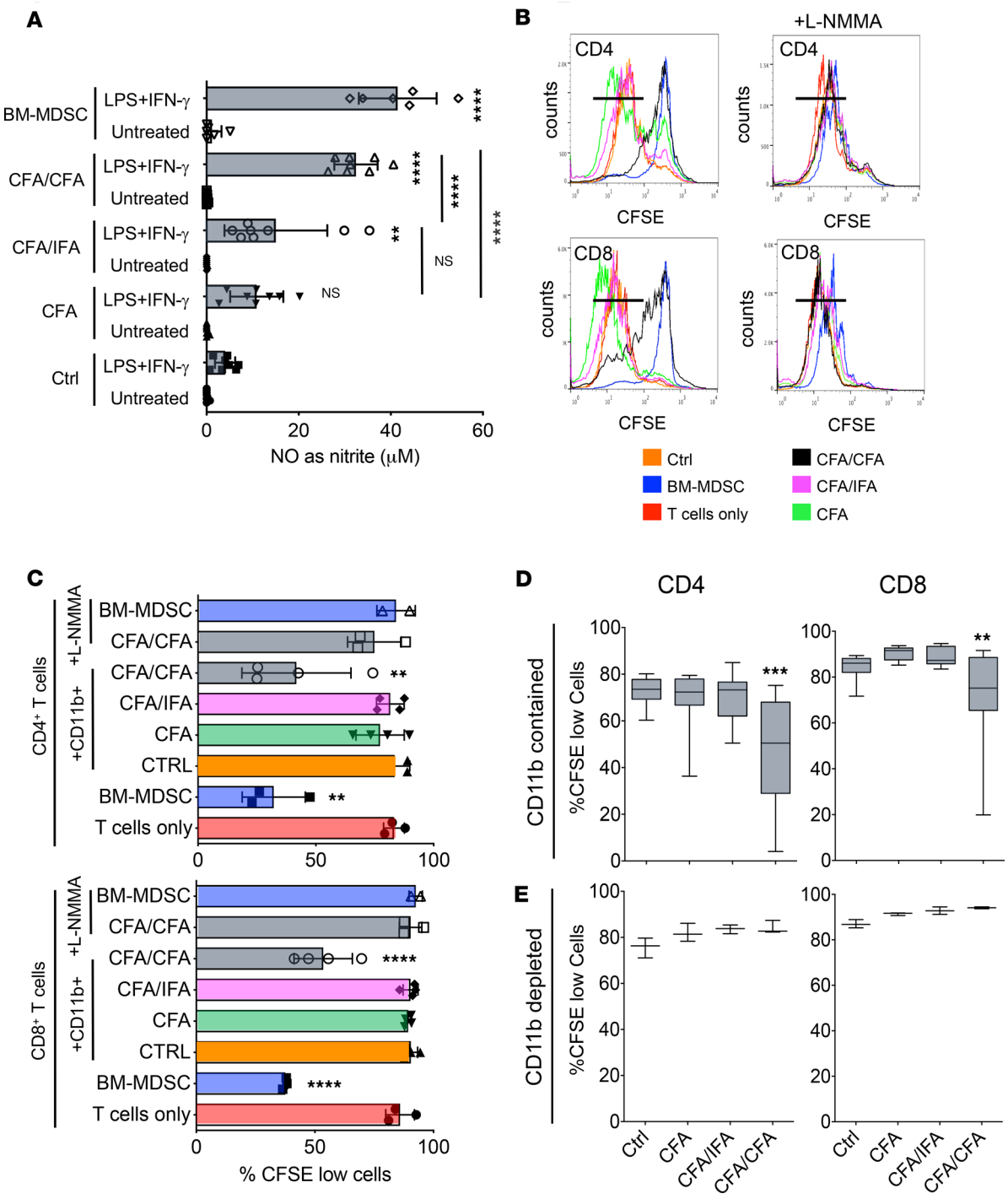

Figure 2. Only CD11b⁺ cells isolated from CFA/CFA mice produce substantial amounts of NO and suppress T cell proliferation. (**A**) CD11b⁺ cells from spleen cells of untreated (Ctrl) and CFA-, CFA/IFA-, and CFA/CFA-treated mice were isolated by MACS and compared with in vitro–generated BM-MDSCs for their NO production by Griess assay after overnight stimulation with LPS/IFN-γ. Values correspond to NO production by 2×10^5 cells (3 independent experiments with $n = 8$ replicates, except BM-MDSCs with $n = 6$). (**B**) T cell suppression assays. CFSE-labeled bulk T cells isolated from naive mice were stimulated with CD3/CD28 antibodies and cultured for 4 days with MACS-purified CD11b⁺ cells from untreated and CFA-, CFA/IFA-, and CFA/CFA-treated mice or in vitro BM-generated MDSCs in the presence or absence of L-NMMA. Example assay showing the gating for proliferated CFSE^{lo} cells. (**C**) Pooled data of individual experiments, as shown in **B**, are displayed. For T cells only, BM-MDSC, CFA/CFA plus L-NMMA ($n = 3$). For CTRL, CFA, CFA/IFA, CFA/CFA ($n = 4$). For BM-MDSC plus L-NMMA ($n = 2$). (**D**) Ex vivo bulk T cell proliferation assay. Spleens from untreated (Ctrl, $n = 14$ mice), CFA- ($n = 16$), CFA/IFA- ($n = 15$), and CFA/CFA-treated mice ($n = 16$) were CFSE labeled and then stimulated with CD3/CD28 antibodies for 4 days. The percentages of proliferated CFSE^{lo} cells within the CD4⁺ and CD8⁺ T subsets are shown. (**E**) Ex vivo bulk T cell proliferation assay. CD11b⁺ cell–depleted spleens from untreated and CFA-, CFA/IFA-, and CFA/CFA-treated mice ($n = 3$) were CFSE labeled and then stimulated with CD3/CD28 antibodies for 4 days. The percentages of proliferated CFSE^{lo} cells within the CD4⁺ and CD8⁺ T subsets are shown. Statistical significance was assessed by comparison of sorted cells from control versus treated mice (**A**) or T cells only versus T cells cocultured with ex vivo–sorted CD11b⁺ cells from treated mice (**C**) or bulk splenic T cells from control versus treated mice (**D** and **E**). Statistics by 1-way ANOVA with multiple comparisons and Tukey's post test. $^{**}P < 0.01$,$^{****}P < 0.0001$.

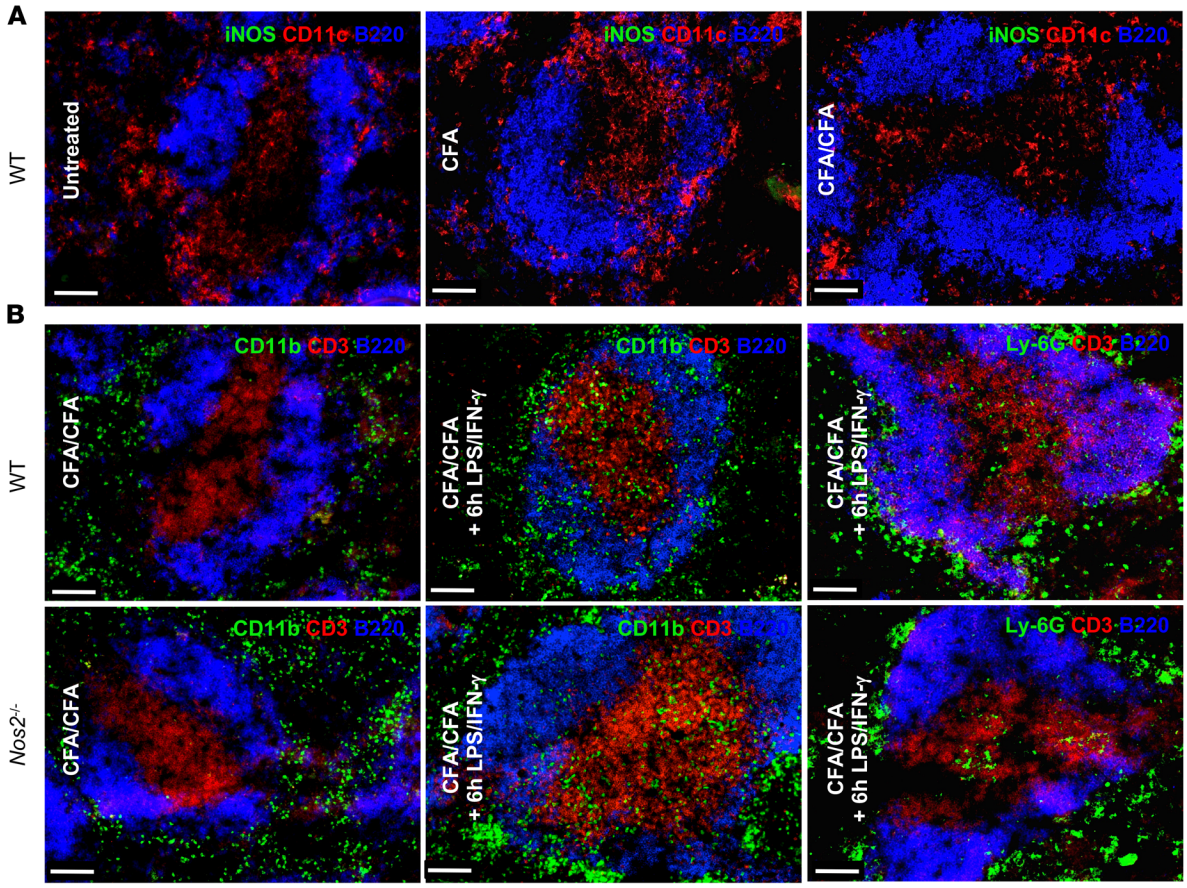

Figure 3. Systemic LPS/IFN-γ administration induces MDSC infiltration into the splenic white pulp. (**A**) Spleens from untreated (Ctrl) and CFA- and CFA/CFA-immunized mice were collected after 15 days, and cryosections were stained for iNOS, B220, and CD11c. (**B**) WT and *Nos2*$^{-/-}$ mice were CFA/CFA injected and challenged with i.p. LPS/IFN-γ administration for 6 hours. Then spleens were stained for B220, CD11b, Ly6G, and CD3 as indicated. All microscopy data are representative of 3 independent experiments (n = 3 mice). Scale bars: 100 μm.

Surprisingly, higher resolution microscopy revealed that iNOS$^+$ cells were closely associated with CD11c$^+$ DCs in the T cell areas and partially seemed to form synapses (Figure 4C). Counterstaining with CD115 identified the iNOS$^+$ cells in spleen sections of CFA/CFA plus LPS/IFN-γ–injected mice as monocytic cells, which appeared either as iNOS^{bright} cells in the marginal zone and bridging channels (Figure 4D, BC and MZ) or as iNOS^{dull} cells in the T cell areas (Figure 4E, T).

Together, these findings indicate that LPS/IFN-γ challenge induces a rapid accumulation of granulocytic and monocytic cells into the T cell areas after 6 hours. iNOS$^+$CD115$^+$ M-MDSCs releasing NO especially localize close to CD11c$^+$ DCs. Substantial M-MDSCs infiltration and iNOS detection was restricted to mice that were preimmunized with the CFA/CFA protocol, while a single CFA or CFA/IFA immunizations or LPS/IFN-γ challenge did not show this effect. It remained to be determined whether the appearance of iNOS$^+$ M-MDSCs in the T cell areas had functional consequences.

NO-dependent DC killing by M-MDSCs in the splenic T cell areas of CFA/CFA-immunized mice. We tested whether the observed iNOS$^+$ M-MDSC infiltration of the splenic T cell areas led to changes in the absolute numbers of T cells or DCs as an indicator of killing. We counted the cell numbers of DCs and T cells in spleens of CFA/CFA-immunized mice that were challenged for the established iNOS-inducing LPS/IFN-γ treatment or *M. tuberculosis*/IFN-γ. The CD11c^{hi}MHC-II^{hi} B220$^-$ cDCs numbers continuously decreased over 48 hours. In contrast, the numbers of CD11c$^+$B220$^-$ pDCs and both CD4$^+$ and CD8$^+$ T cell subsets increased over 48 hours under both challenge conditions (Figure 5A). Since apoptosis needs to be measured before the disappearance of cells, we restricted further experiments to the earlier time points.

Splenic DC and T cell populations were analyzed by FACS for the appearance of apoptotic cells, as detected by annexin V binding. After 24 hours, but not 6 hours, the frequency of apoptotic annexin V$^+$

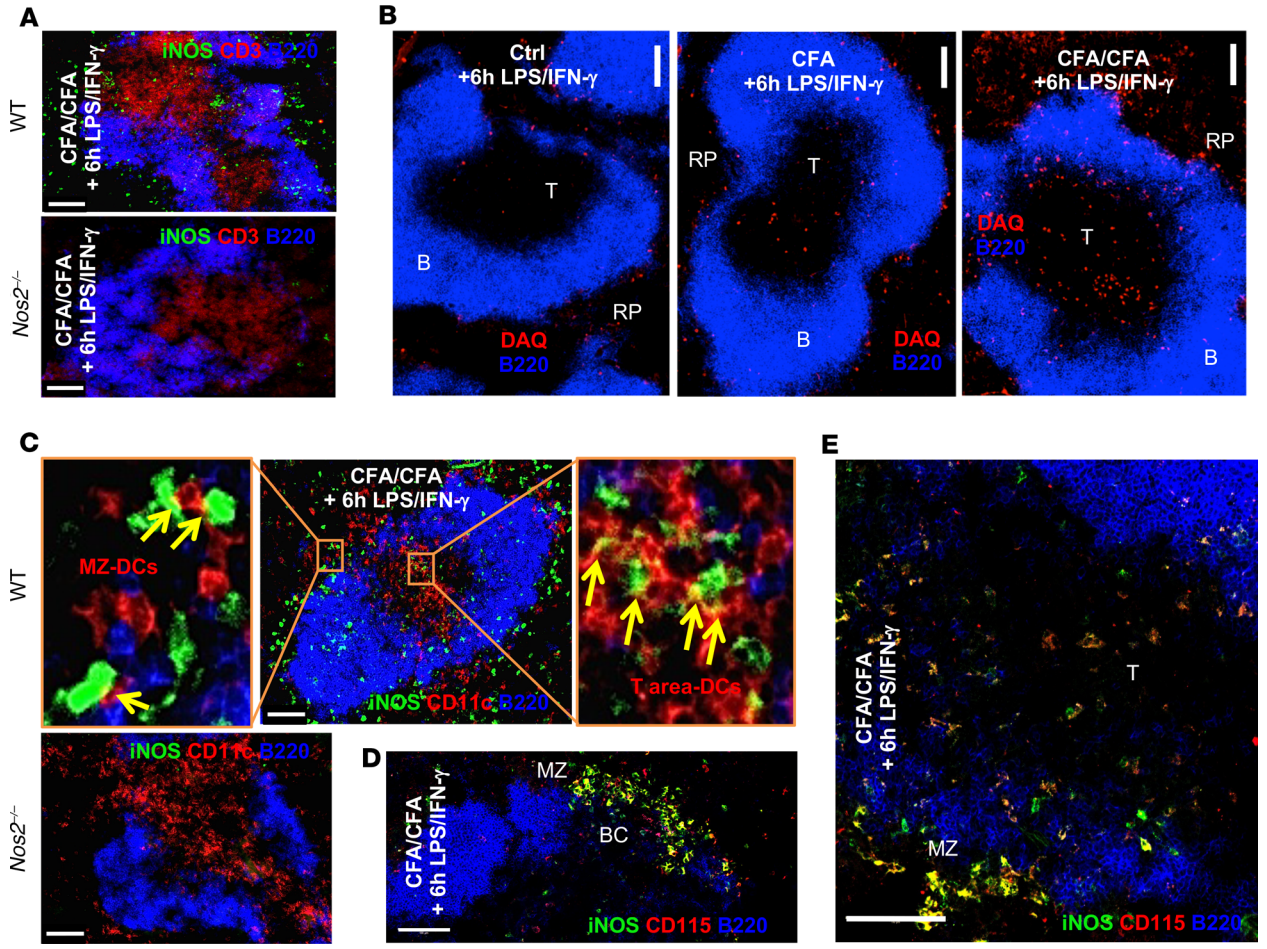

Figure 4. Systemic LPS/IFN-γ administration induces iNOS and NO production by CD115⁺ M-MDSCs interacting with CD11c⁺ DCs. (**A**) WT and *Nos2*$^{-/-}$ mice were injected as in Figure 3B but stained for B220, iNOS, CD11c, and CD3 markers as indicated or (**B**) with B220 and the NO-detecting reagent DAQ. T, T cell areas; B, B cell areas. (**C**) WT and *Nos2*$^{-/-}$ mice were injected with CFA/CFA plus 6-hour LPS/IFN-γ. The spleen sections were stained with B220, CD11c, and iNOS. Enlarged areas show marginal zone DCs (MZ-DCs) or DCs in the T cell area (T area-DCs) in close contact or forming synapse-like structures with iNOS⁺ cells. (**D** and **E**) Mice treated, as in **B**, stained with iNOS, B220 and CD115. BC, bridging channel; MZ, marginal zone. All microscopy data are representative of 3 independent experiments (n = 3 mice). Scale bars: 100 μm.

cDCs and annexin V⁺ pDCs substantially increased (Figure 5B). Systemic LPS-IFN-γ challenge without prior CFA/CFA immunization did not reveal any increase in apoptosis of cDCs, while it partially induced apoptosis in pDCs (Figure 5B, violet). Interestingly, none of these conditions increased CD4⁺ and CD8⁺ T cell apoptosis at both time points, while an antiapoptotic effect appeared in CD8⁺ T cells at 6 hours and only in *Nos2*$^{-/-}$ mice (Figure 5B). The antiapoptotic effect may result from the observed DC maturation after LPS/IFN-γ injection (Supplemental Figure 4A), which resulted in increased T cell activation (Supplemental Figure 4B), lending at least a transient antiapoptotic effect to the T cells.

To substantiate these findings, we determined the frequencies of the same cell populations in the spleen. The cDCs frequencies were diminished at both 6 hours and 24 hours in WT mice but not in *Nos2*$^{-/-}$ mice. At the same time, the frequencies of pDCs relatively increased, despite increased frequencies of apoptotic cells (Figure 5C). This, together with the higher absolute cell number of pDCs, may suggest a simultaneous killing by MDSCs but also enhanced recruitment of pDCs into the spleen, such as observed after viral infections (30).

Importantly, both reduced frequencies and increased apoptosis occurred for *Nos2*-dependent cDCs after LPS/IFN-γ injection, and a similar trend was observed with *M. tuberculosis*/IFN-γ, but only transiently after 24 hours. Circulating cells, such as pDCs and CD4⁺ and CD8⁺ T cells, remained stable in their frequencies or were moderately increased. While pDCs showed increased apoptosis, T cells seemed not to be affected (Figure 5C). Thus, LPS/IFN-γ injection induced preferential cDC and pDC killing but spared T cells.

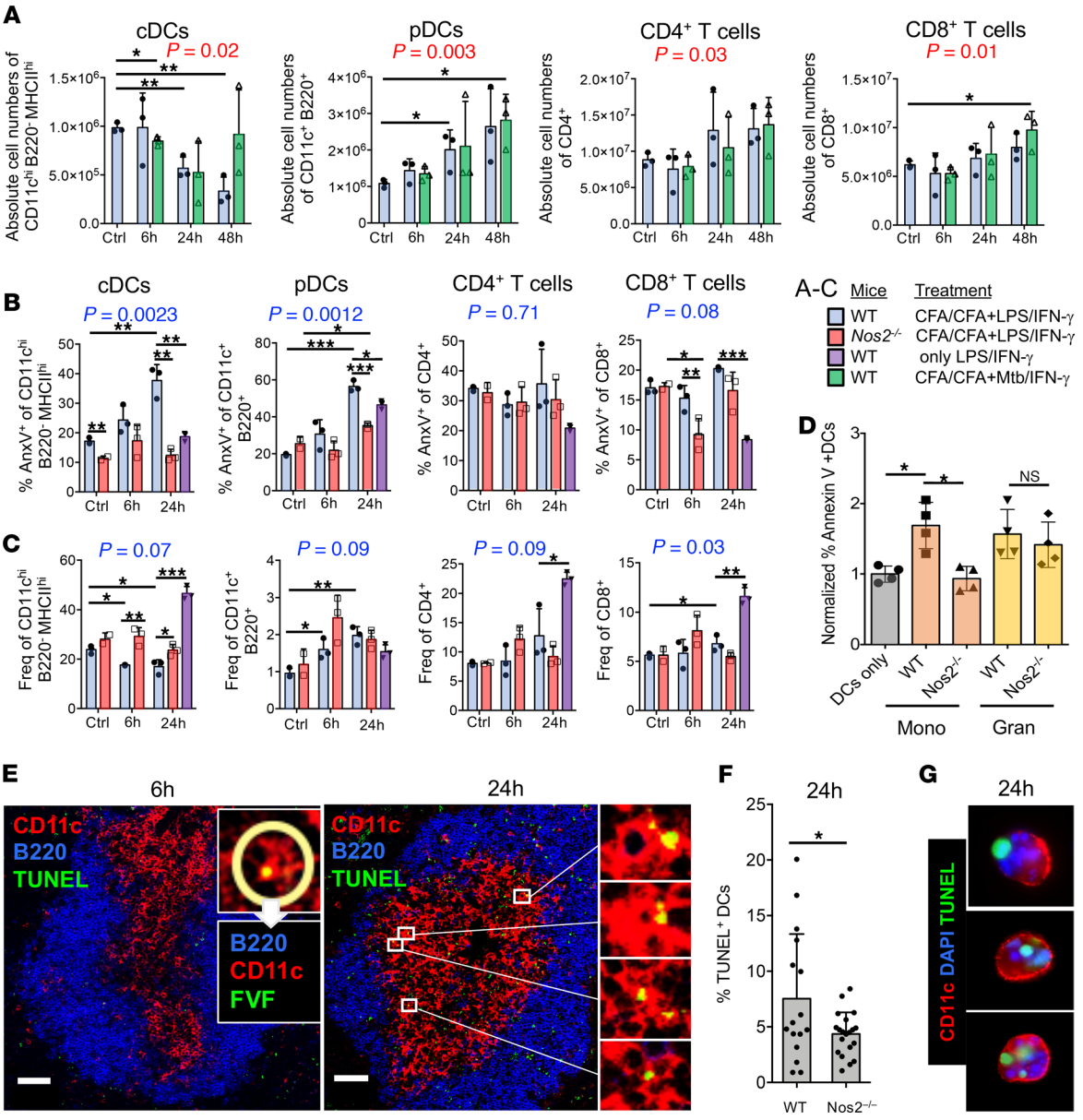

Figure 5. MDSC-mediated DC killing is iNOS dependent. (**A**) C57BL/6 WT mice (n = 3) were immunized s.c. with CFA/CFA or were left untreated (without CFA) and challenged with LPS/IFN-γ, *M. tuberculosis*/IFN-γ, or vehicle (0h). Spleens were harvested after 6 hours, 24 hours, and 48 hours after the mice received the challenge injections, and the absolute cDC, pDC, and CD4$^+$ and CD8$^+$ T cell numbers were calculated from the frequencies of the indicated surface marker stainings among the whole spleen cell counts. (**B**) C57BL/6 WT (n = 3) and *Nos2*$^{-/-}$ mice (n = 3) were used for immunization as above but only challenged with LPS/IFN-γ. The individual cell populations were stained using the indicated markers and analyzed by flow cytometry after 6 hours and 24 hours for the frequency of apoptotic cells using annexin V or (**C**) their live-cell frequencies were calculated. (**D**) DC in vitro killing assay. In vitro–generated BM-DCs were matured overnight with LPS and then cocultured at 1:1 ratio with *M. tuberculosis*–activated BM-MDSCs that were generated from WT or *Nos2*$^{-/-}$ mice and sorted into CD11b$^+$Ly6C^{hi}Ly 6G$^-$ monocytic or CD11b$^+$Ly6C^{lo}Ly6G$^+$ granulocytic cell subsets (n = 4 independent experiments). Apoptosis of DCs was determined by annexin V FACS staining and normalized to DC cultures without BM-MDSCs. (**E**) Cryosections of spleens from CFA/CFA plus LPS/IFN-γ–immunized mice were analyzed by confocal microscopy to assess apoptosis of CD11c$^+$ DCs via TUNEL or FVF staining. B cell areas were identified by B220 staining. Scale bars: 60 μm. (**F**) Quantification of **E** at 24 hours. CD11c$^+$TUNEL$^+$ cells within the T cell zone of WT (n = 16) and *Nos2*$^{-/-}$ (n = 20) spleen cryosections were analyzed with StrataQuest software. (**G**) Cytospin preparations of LPS-matured BM-DC and *M. tuberculosis*–activated BM-MDSC cocultures to demonstrate CD11c$^+$TUNEL$^+$ DC killing in vitro. Statistics shown in black were performed using an unpaired 2-tailed t test. *P < 0.05, **P < 0.01, ***P < 0.001. Mean and SD are shown. Statistical P values shown in red were performed using 2-way ANOVA testing for changes over time, while no differences were found between the differentially treated groups. Statistical P values shown in blue were performed using 2-way ANOVA testing for changes over time and between the WT and *Nos2*$^{-/-}$ mice. ANOVA analyses were performed without the group that received only LPS/IFN-γ (violet bars).

BM-MDSC–mediated BM-DC killing in vitro. NO-mediated suppression and induction of apoptosis of T cells are among findings frequently reported as mechanisms of M-MDSC function (31), findings which are also supported by our ex vivo data. Conversely, DC killing had not been reported in vitro. Therefore, we set up a series of in vitro assays to study the effect of *M. tuberculosis* on in vitro–generated M-MDSCs and on their effects on DCs and T cells.

MDSCs generated from murine BM with GM-CSF (BM-MDSCs) by our established protocol (20) recapitulated iNOS induction and NO production upon *M. tuberculosis* stimulation, which can be attributed mostly to M-MDSCs and to a much lesser extent to G-MDSCs, and increased suppression of T cell proliferation, all effects that were similar to those after LPS/IFN-γ stimulation (Supplemental Figure 2) and as observed previously (22). BM-MDSCs prevented CD25 upregulation, modified CD69 expression, and finally induced T cell apoptosis in vitro in an *Nos2*-dependent manner (Supplemental Figure 3). Thus, T cell suppression and apoptosis can be readily demonstrated in vitro and ex vivo but not in our in vivo settings.

To address DC killing in vitro, *M. tuberculosis*–activated BM-MDSCs were sorted into granulocytic or monocytic subsets of WT mice and *Nos2*$^{-/-}$ mice and cocultured with LPS-matured BM-DCs. Only the monocytic BM-MDSC subset induced *Nos2*-dependent apoptosis of DCs (Figure 5D). Similarly, LPS/IFN-γ–activated BM-MDSCs but not unstimulated MDSCs induced apoptosis of LPS- or CpG oligonucleotide–matured BM-DCs in an iNOS-dependent manner, since the NO-inhibitor L-NMMA reverted apoptosis, as shown for annexin V by FACS (Supplemental Figure 5A) or TUNEL staining by confocal microscopy (Supplemental Figure 5B). These data indicate that the *M. tuberculosis*– or LPS/IFN-γ–activated M-MDSCs subset within BM-MDSCs can directly kill BM-DCs by release of NO in vitro, supporting our in vivo findings.

DC killing in the T cell areas detected in situ. To corroborate the DC killing data obtained so far, we further performed immunofluorescence staining of the spleens. TUNEL staining detecting apoptosis at a relatively late stage did not reveal any dead cells at 6 hours in the spleen (Figure 5E). Using an earlier apoptosis marker, FAM-VAD-FMK (FVF), we found individual CD11c$^+$ cells that appeared with a positive nuclear staining, but these cells were too few for further statistical evaluation (Figure 5E, 6h inset). In contrast, after 24 hours TUNEL$^+$ cells were readily detectable in the T cell areas of spleens in CFA/CFA plus LPS/IFN-γ–injected mice (Figure 5E). To quantify DC apoptosis in the T cell areas, we used StrataQuest software with the same markers and costained T cells obtained from splenic sections of WT and *Nos2*$^{-/-}$ mice by TUNEL (32). Indeed, a substantial proportion of spleen sections showed increased frequencies of CD11c$^+$TUNEL$^+$ cells in the T cell areas at 24 hours. This was not observed in sections from *Nos2*$^{-/-}$ mice, suggesting the induction of NO-dependent DC apoptosis in T cell areas of the spleen (Figure 5F). Since TUNEL$^+$ spot staining did not seem to clearly colocalize with CD11c$^+$ cell nuclei (Figure 5E, 24h, enlarged areas), as we had detected by FVF staining at 6 hours (Figure 5E, inset), we sought to confirm this apoptosis pattern by TUNEL staining with BM-DCs cocultured with activated BM-MDSCs for 24 hours in vitro. The in vitro–cultured apoptotic BM-DCs showed a similar pattern of TUNEL$^+$ spots, which also did not fully colocalize with the nuclear DAPI staining (Figure 5G). Therefore, this 24-hour TUNEL staining pattern is compatible with the detection of apoptotic bodies under in vivo conditions.

Together, our results indicate that pathogen-activated MDSCs rapidly infiltrate into the splenic T cell areas in CFA/CFA-immunized mice within 6 hours. After 24 hours iNOS-dependent induction of apoptosis of cDCs and pDCs can be observed. Surprisingly, CD4$^+$ and CD8$^+$ T cell apoptosis was not detectable in any of our in vivo conditions.

Discussion

Here, we addressed the question of whether an IFA-based vaccine equivalent to human adjuvant Montanide ISA-51 VG that containing additional heat-killed *M. tuberculosis* (together called CFA) can induce functional MDSCs in mice. We found accumulating monocytic and granulocytic cells in the splenic red pulp after single CFA as reported previously (7, 19) but even more after CFA/CFA double immunizations. Functionally, only CD11b$^+$ cells from spleens of CFA/CFA but not otherwise immunized mice acquired NO-producing capacity and iNOS-dependent T cell suppressor activity after stimulation ex vivo, indicative of MDSC induction. While iNOS expression or NO production was not detectable in situ in CFA/CFA-immunized mice, both could be activated by 6 hours after LPS/IFN-γ injection. This indicates that monocyte licensing for suppression had occurred in the spleen by the CFA/CFA treatment, but no activation from L-Mono into M-MDSCs had occurred yet. These results are compatible to what we found before in vitro (21, 22). Both granulocytic and monocytic cells infiltrated the white pulp

T cell areas, but only CD11b$^+$ CD115$^+$ monocytic cells were counterstained as iNOS$^+$. This phenotype is compatible with M-MDSCs (1). As a result of the LPS/IFN-γ or *M. tuberculosis*/IFN-γ injections, we could observe NO-dependent apoptosis of cDCs and pDCs while T cells seemed unaffected.

While CFA is a potent adjuvant, our data indicate that it can also induce immunosuppressive M-MDSCs when administered twice. While previous reports indicated suppressive effects of CD11b$^+$ cells already after a single application of 100 μL CFA on ConA-stimulated T cells (7, 19), we could not observe this using half the dose to avoid open skin wounds at the injection site and by stimulating T cells with anti-CD3/CD28 antibodies. Importantly, the *M. tuberculosis* content within the second CFA vaccine determined the immunological outcome, as demonstrated by the failure of the CFA/IFA injection protocol to generate NO-producing cells and to confer suppressor potential to CD11b$^+$ myeloid spleen cells. Although the splenic infiltrates into the T cell areas after LPS/IFN-γ injection in CFA/CFA mice and bulk cultures of BM-MDSCs contained monocytic and granulocytic cells, we identified the M-MDSCs as primary NO producers and suppressor cells and did not further address the granulocytic subset. The granulocytic MDSC infiltration into the T cell areas may have a partial role for NO in DC killing, but a clear understanding of their function within the T cell areas requires further investigation.

The data obtained here follow the same 2-step rules for licensing and activation of MDSCs as described before (21, 22). As a critical first step, the conversion of classical Ly6C^{hi} monocytes into L-Mono was identified as a prerequisite for the acquisition of M-MDSC suppressor function. In our system, GM-CSF–mediated monocyte licensing was identified as a critical component for subsequent M-MDSC generation (21). GM-CSF is a generally accepted inducer of MDSCs (2). Others have shown that *M. tuberculosis* components increased the serum GM-CSF levels when injected into mice (33) and that TB patients show elevated GM-CSF levels in pleural effusions similar to those of tumor patients (34). In this study, the expansion of the myeloid cells was observed in spleens of CFA-injected mice. However, we did not assess whether *M. tuberculosis* release from CFA and its transport to the BM can directly promote myelopoiesis or whether *M. tuberculosis* induces indirectly myeloid cell expansion or monocyte licensing by inducing a myeloid growth factor. An indirect stimulatory effect of pathogen components, such as β-glucan on GM-CSF and IL-1β–induced proliferation of early hematopoietic cells, has been reported to induce trained immunity (35). BCG infection can induce metabolic changes in monocytes associated with trained immunity (36). However, changes observed as monocyte training were found not to act directly on differentiated monocytes but to occur by epigenetic modifications on early myeloid precursors, which then result in trained monocytes (35, 37). This BCG-mediated training effect resulted in a better secondary innate immunity against viral infection, which correlated with IL-1β upregulation, while GM-CSF was not investigated (38). If pathogens induce epigenetic modifications at the chromatin level, then the use of histone deacetylase (HDAC) inhibitors may allow a switch from monocyte training toward MDSC development. In fact, in vitro the GM-CSF–mediated BM precursor development into monocytic BM-DCs was blocked by the HDAC inhibitor trichostatin A and resulted in NO-producing M-MDSCs (39). Whether *M. tuberculosis* vaccination can also induce chromatin modifications and how such epigenetic modifications and their inhibition may balance the GM-CSF–dependent trained monocyte or M-MDSC generation requires further in vivo investigations.

It is unclear whether epigenetic modifications induced by *M. tuberculosis* are restricted to myeloid precursors or whether they can also occur in differentiated monocytes. Again, in vitro evidence suggests that the late developmental switch from differentiated human CD14$^+$ monocytes into either macrophages or DCs is directed by epigenetic changes (40). We found previously that in GM-CSF differentiated BM-MDSC cultures, transcriptional and translational changes occur that are prerequisite for their development into M-MDSCs (21). Thus, it is tempting to speculate that, in *M. tuberculosis*–induced M-MDSC generation, epigenetic changes also can occur at a differentiated monocyte stage.

Previously we demonstrated that proinflammatory cytokines (21) or systemic LPS/IFN-γ administration in mice (22) can serve as factors for the second activation step that converts L-Mono into M-MDSCs. Here, we found that also *M. tuberculosis*/IFN-γ injections could induce DC killing, although to a lesser extent. We believe that this reduced efficiency is due to the whole bacteria *M. tuberculosis* preparation and that standardized smaller particles or defined soluble components as available in *M. tuberculosis* vaccines for clinical studies may reveal more clear results.

The IFN-γ component of our challenging protocol appears as a major component of MDSC activation, and blocking by antibodies or genetic deficiency of the receptor largely abrogates MDSC activation of NO production (21, 22). In TB infection, the *M. tuberculosis* challenge may directly occur in the lung or after

bacterial dissemination to the spleen and other sites. In such a scenario, infiltrating NK cells or effector T cells may typically account for local IFN-γ production.

Injection of LPS/IFN-γ induced MDSC accumulation in T cell areas. Since this process occurred very rapidly, we presume that MDSC infiltration starts from the red pulp and bridging channels and not by recruitment from the BM. Such an intrasplenic translocation has been observed before for DCs that moved from the bridging channels to the white pulp after LPS injection into mice (41), and DC homing into the splenic T cell areas was proposed to depend on CCR7 (42), similar to lymph nodes. However, lymph node homing of MDSCs is poor in most animal models investigated (43, 44), and FACS analysis of spleen MDSCs after CFA/CFA plus LPS/IFN-γ treatment did not reveal CCR7 expression (data not shown), indicating that other homing receptors may mediate this effect.

Induction of T cell apoptosis by MDSCs via NO production belongs to the earliest suppressor mechanisms that have been described for MDSCs in vivo (4, 45) and is now considered as a prominent mechanism for MDSC-mediated suppression (1, 46). However, MDSC-derived NO has been demonstrated to affect T cells mainly in vitro or ex vivo, such as by restimulation of spleen cells from *Trypanosoma*-infected mice (47). In our study, suppression of CD3/CD28 antibody-induced T cell proliferation and apoptosis in vitro and ex vivo was entirely dependent on the NO-dependent mechanism, as shown by the use of the L-NMMA inhibitor or *Nos2*-deficient MDSCs. From these in vitro and ex vivo findings it had been extrapolated that the abrogation of suppressor function in mice by injection of L-NMMA or the use of *Nos2*$^{-/-}$ mice must rely on the direct suppression of M-MDSCs on T cells, although this had not been formally proven. Our data indicate that although NO-dependent T cell apoptosis can be readily observed in vitro, apoptotic CD4$^+$ or CD8$^+$ T cells were not found in our setting in vivo, both after CFA/CFA immunizations alone or with additional LPS/IFN-γ challenge. Since the clearance of apoptotic cells is highly efficient and T cells are continuously circulating, it may well be possible that we missed the detection of T cell apoptosis. We also cannot exclude the presence of a low frequency of activated *M. tuberculosis*–specific T cells as specific targets of M-MDSC suppression within the general pool of all and mostly resting T cells. On the other hand, our ex vivo T cell stimulation data showing an impaired proliferation in presence of CD11b$^+$ cells could be fully and immediately reconstituted when CD11b$^+$ cells were removed. This indicates that T cells of CFA/CFA-immunized mice are under reversible suppression of M-MDSCs but may not be deleted by apoptosis.

Instead, we discovered that cDCs and pDCs can be direct targets of iNOS-dependent killing by M-MDSCs in vivo; thus, they represent what we believe to be a novel mechanism of indirect M-MDSC–mediated T cell suppression in addition to the known direct effects on T cells. While CFA/CFA immunization was required for CD11b$^+$ spleen cells to acquire a high NO-producing and T cell suppressive capacity ex vivo, these mice did not show persistence of iNOS$^+$ cells or elevated NO production in the T cell areas 3 days after the last CFA injection. However, DC apoptosis was detected after a short-term systemic LPS/IFN-γ and to a lesser extent after *M. tuberculosis*/IFN-γ challenge. M-MDSCs were recruited into the white pulp T cell area, in which they seek close contacts with DCs after 6 hours and finally induced cDC and pDC apoptosis after 24 hours. Importantly, cDCs did not and pDCs did only partially die from apoptosis by the LPS/IFN-γ treatment alone. DC apoptosis was abrogated in *Nos2*$^{-/-}$ mice, as observed via annexin V binding by FACS and detected by TUNEL staining in splenic cryosections. Our in vitro data also indicated that BM-DCs could be killed by M-MDSCs through apoptosis induction by NO. Together, our data demonstrate for the first time to our knowledge iNOS-mediated suppressor effects of MDSCs in vivo. In addition to the iNOS-dependent killing on T cells that could be observed in vitro and ex vivo, these in vivo results now demonstrate mycobacteria-induced iNOS-dependent killing of DCs.

Our results regarding the abrogation of adjuvant effects in CFA/CFA mice may relate to human TB vaccination studies. BCG revaccinations are not recommended anymore due to a lack of additional protective effects (48). The induction of MDSCs was not investigated in these individuals. In contrast, boosted T cell responses could be observed when an Ag85A *M. tuberculosis* subunit vaccine was applied within a human adenovirus 5 vector after a BCG prevaccination (49). These findings may indicate that either whole mycobacteria are required to induce MDSCs or that specific subcomponents may lack this ability. Alternatively, the subsequent use of antigens from 2 different mycobacterial species as vaccines may somehow blur a pathogen-specific MDSC induction. In a recent study, adolescents revaccinated with BCG or H4:IC31 (containing the TB10.4 and Ag85A *M. tuberculosis* antigens) after they received BCG vaccination during infancy, showed boosted CD4$^+$ T cell responses within PBMCs when restimulated with vaccine antigens in vitro in the BCG revaccination group (50). These results may indicate that a longer time period between

first (infancy) and second (adolescence) vaccination may be beneficial for boosting T cell responses out of bulk PBMCs as compared with our prime/boost regimen with an interval of only 12 days.

In conclusion, our data suggest that a single vaccination with dead *M. tuberculosis*, such as performed here with CFA, induces a similar MDSC accumulation in the spleen as observed before in the draining lymph nodes and blood after live s.c. BCG injection into mouse ears (23). We found that a single CFA injection or a CFA/IFA sequence of injections still shows intact T cell proliferation in the spleen in accordance to the well-described adjuvant effects of CFA, while others observed local suppressive effects in skin and lymph nodes using single live BCG injections (23). While after live BCG immunization, a clear Ly6C^{hi} population was not distinguishable from the general Ly6C^{+} monocytic cell pool, the functional consequences of BCG or *M. tuberculosis* vaccinations are very similar in their NO-dependent suppressive effect on T cells, dampening the in vivo priming (23), consistent with induction of the M-MDSC subset. In our case, only repeated CFA vaccination fully activated MDSC suppressor activity at a systemic level. This delay or weaker MDSC development is potentially due to the use of dead material instead of live bacteria. While MDSC infection by BCG (23) and *M. tuberculosis* (11) has been observed, we can exclude live bacterial dissemination to the spleen and rather indirect effects may have mobilized splenic MDSC accumulation in our experimental setting. As a potentially novel suppressor mechanism, we identified NO-dependent DC killing in the splenic white pulp T cell areas. Since impaired memory T cell generation and lack of protection have been found also in experimental *M. tuberculosis* infections of mice (11) and in human TB patients (9, 10), our findings in mice may have implications for TB vaccinations in humans and suggest that investigations on potential MDSC induction and DC killing also in human trials should be considered.

Methods

Mice. C57BL/6J (Charles River) and *Nos2*$^{-/-}$ (B6.129P2-*Nos2*^{tm1Lau}/J, The Jackson Laboratory) mice were bred in our animal facilities, kept under specific pathogen–free conditions, and used at an age of 7–12 weeks.

In vivo treatment of mice. C57BL/6 mice were injected s.c. into the flanks with 100 μL CFA/PBS emulsions at a 1:1 ratio. The CFA was further enriched with *M. tuberculosis* as described for myeloid cell expansion (51). Revaccination was performed s.c. either with 50 μL IFA/PBS emulsion or 50 μL CFA/PBS emulsion. For some experiments, mice were injected with 10 μg LPS plus 1 μg IFN-γ i.p. for 6 hours or 24 hours or 10 μg sonicated heat-killed *M. tuberculosis* (Difco) plus 1μg IFN-γ to provoke iNOS induction.

Cell preparation. BM-MDSCs and BM-DCs were generated as described previously (20, 52). Briefly, BM cells from C57BL/6 mice were seeded at 3×10^6 per 100 mm petri dish (Greiner) in 10 mL of fresh RPMI1640 medium (PAA) containing 10% heat-inactivated FCS from GIBCO (termed R10), supplemented with 100 U/mL penicillin (MilliporeSigma), 100 μg/mL streptomycin (MilliporeSigma), 2 mM L-glutamine (MilliporeSigma), 50 μM β-mercaptoethanol (MilliporeSigma), and 10% GM-CSF supernatant (53). BM-MDSCs were used at day 3 for assays. Murine BM-DCs were generated in the same way, but on day 3 of culture, 10 mL complete RPMI medium supplemented with 10% GM-CSF–containing supernatant was added. On day 6, 10 mL of the medium was removed, and fresh medium was added as at day 3. BM-DCs were used at day 7–8 of culture.

Reagents. GM-CSF was obtained from supernatant of cell lines transfected with the murine GM-CSF gene (53). IFN-γ (0.5 μg/mL) was purchased from Immunotools. CFA/IFA, LPS (1 μg/mL), N^{G}-Methyl-L-arginine acetate salt (L-NMMA, 500 μM) and 1,2-Diaminoanthraquinone (DAQ, 10 μM) were purchased from MilliporeSigma. Killed and dried *M. tuberculosis* (H37Ra strain) was purchased from Difco. All concentrations were used as indicated in the figures or legends.

Flow cytometry. The murine directly conjugated antibodies CD11b-PerCP-Cy5.5 (M1/70), CD11b-APC (M1/70), B220-Pacific Blue (RA3-6B2), Gr-1-Alexa Fluor 647 (RB6-8C5), Ly6G-PerCP-Cy5.5 (1A8), Ly6G-APC/Fire (1A8), Ly6C-Alexa Fluor 647 (HK1.4), Ly6C-Brilliant Violet 510 (HK1.4), CD4-APC (GK1.5), CD4-PerCP-Cy5.5 (GK1.5), CD8-PerCP-Cy5.5 (53-6.7), CD8-APC (53-6.7), CD11c-PE-Cy7 (N418), CD25-FITC (PC61), CD69-Alexa Fluor 488 (H1.2F3), CD69-APC (H1.2F3), Streptavidin Brilliant Violet 421, and annexin V-FITC were all purchased from Biolegend. Propidium iodide was purchased from R&D System. iNOS-PE (CXNFT) was obtained from eBioscience.

Cells were stained in PBS containing 0.1% BSA, 0.1% sodium azide, and 5% fetal bovine serum in the dark for 30 minutes on ice. For intracellular iNOS detection, cells were first labeled for surface markers and then washed and subsequently fixed with 2% PFA for 10 minutes at room temperature. Cells were next permeabilized and stained with FACS buffer containing saponin (0.5%) for 1 hour at 4°C together with the marker-specific antibody. Samples were washed once in staining buffer and measured with a FACS Calibur or LSR II (Becton Dickinson). Results were analyzed with FlowJo software (Tree Star).

Cytospins, tissue staining, and microscopy analysis. For visualization of the in vitro DC killing assay, 24- or 48-hour cocultured cells were collected and washed and 5×10^5 cells were deposited onto a poly-L-lysine–coated glass slide (Poly-Prep, MilliporeSigma) and allowed to precipitate for 1 hour at 37°C. Cells were next fixed in 2% PFA for 10 minutes at room temperature, washed twice in PBS, and blocked and permeabilized in PBS containing 2% goat serum with 0.1% Triton X-100 and 0.1% BSA for 20 minutes at room temperature. The primary antibody CD11c-Alexa Fluor 594–conjugated (clone N418, Biolegend) was diluted 1:100 in PBS and incubated overnight at 4°C. Slides were washed several times in PBS and TUNEL assay was subsequently performed (see below) for the detection of apoptotic cells. Nuclei were stained using DAPI (AppliChem). Spleens from euthanized mice were collected and transferred into tubes containing OCT compound (Tissue-Tek, SAKURA), immediately frozen, and stored at (–80°C). Organs were subsequently cut into 10-μm-thick slices using a Cryotome (Leica), and tissue was stained using the same procedure and buffers described for the cytospin cells. Finally, slides were repeatedly washed in PBS, dried, and mounted with Fluoromount-G (SouthernBiotech). Tissue sections were all visualized and further analyzed with an Imager.Z1m immunofluorescence microscope (Zeiss). Primary antibodies used for tissue cell detection were as follows: Gr-1-Biotin (RB6-8C5) and CD11b-Biotin (M1/70) was purchased from BD; CD11b-Alexa Fluor 488 (M1/70) was obtained from Serotec; F4/80-Alexa Fluor 488 was purchased from Bio-Rad; and CD45R/B220-Alexa Fluor 647 (RA3-6B2), Ly6G-purified (1A8), CD115-Biotin (AFS98), and CD11c-Biotin (N418) were purchased from Biolegend. A polyclonal iNOS antibody was used at 1:20,000 dilution (54). Secondary antibodies Goat anti-Rat IgG DyLight 549 and Streptavidin DyLight 549 were obtained from Rockland; Goat anti-Rat IgG Alexa Fluor 488 and Streptavidin Alexa Fluor 488 were purchased from Life Technologies; Streptavidin Cy3 was obtained from Biolegend; Goat anti-Rabbit IgG DyLight 488 and Goat anti-Rabbit IgG Cy3 were both purchased from Jackson ImmunoResearch. For direct NO detection, DAQ was used (MilliporeSigma, D11582). The frozen tissue was allowed to thaw at room temperature, washed once with 1× PBS, and incubated at 37°C with DAQ in PBS at the concentration of 10 μM for 45 minutes. After washing the slides with PBS, the tissue was costained for other markers (B/T cells), as described before but without fixation and permeabilization steps and at room temperature. Apoptosis was detected by the FVF reagent, a green fluorescent cell-permeable polycaspase inhibitor to target caspase-1, -2, -3, -6, -8, -9, or -10 (AAT Bioquest, ABD-13470; distributor Biomol) or by TUNEL assay (In Situ Cell Death Detection Kit, Roche), both of which were used according to the manufacturers' instructions. Briefly, the samples were stained with Enzyme solution diluted 1:10 with labeling solution (Roche) for 1 hour at 37°C. After 3 washing steps, the slides were embedded in Fluoromount G (SouthernBiotech) and covered with a coverslip. Images were scanned using an LSM 510 Meta Confocal Microscope (Zeiss) and the ZEN Black 8.1 software (Zeiss) and processed via the ImageJ 1.51h software (NIH).

NO measurement. Induction of NO release was performed as described previously by cell stimulation overnight with either IFN-γ (0.5 μg/mL, Peprotech) plus LPS (1 μg/mL, MilliporeSigma) (22) or 50 μg/mL heat-killed *M. tuberculosis* (Difco). NO was measured as nitrite accumulation using the Griess reaction (55). Briefly, 50 μL cell culture supernatant was put into a 96-well ELISA-plate (Corning) as duplicates with titrated $NaNO_2$ (MilliporeSigma) in R10 medium serving as a standard. An aqueous solution of 0.1% naphtylethylendiamine dihydrochloride (MilliporeSigma) and 1% sulfanilamide (MilliporeSigma) in 5% H_3PO_4 (Merck) in water was mixed 1:1, and 50 μL of this solution was added to 50 μL of the samples. The evoked color reaction was measured after 10 minutes in the ELISA reader (Molecular Devices) at 492 nm, and nitrite concentrations were calculated from the sodium nitrite standard curve.

Ex vivo suppressor assay. Organs were processed following standard protocols until single-cell suspensions were obtained. $CD11b^+$ cells were positively sorted by MACS beads and separated through LS columns (Miltenyi Biotec). Sorted cells were tested in a T cell proliferation inhibition assay for their suppressive capacity. Bulk lymph nodes cells from C57BL/6 mice were labeled with CFSE (MilliporeSigma), plated at a fix concentration of 2×10^6 cells in a 24-well plate in 2 mL R10 media, and stimulated with soluble CD3/CD28 antibodies at a final concentration of 2.5 μg/mL. Sorted $CD11b^+$ cells were titrated and added to the T cells at a different ratio. Cells were cocultured over 4 days and their proliferation was measured as CFSE dilution by FACS analysis separately in CD4- and CD8-stained T cell subsets. For the ex vivo bulk T cell proliferation assay, spleens from untreated or treated mice were depleted or not from $CD11b^+$ cells using MACS beads. Splenocytes were then labeled with CFSE and stimulated with soluble CD3/CD28, and their proliferation was measured after 4 days in culture as described above.

In vitro apoptosis assays. Bulk lymph nodes cells from C57BL/6 mice were labeled with eFluor670 (eBioscience), plated at a fix concentration of 2×10^6 cells in a 24-well plate in 2 mL R10 media, and stimulated with soluble CD3/CD28 antibodies at a final concentration of 2.5 μg/mL. L-Mono, as obtained after culture of BM cells for 3 days in GM-CSF, from WT or *Nos2*$^{-/-}$ mice were prepared as described before, titrated, and added to the T cells at a different ratio. Cells were allowed to interact for 24, 48, and 72 hours, and their apoptosis and necrosis induction (annexin V detection and addition of propidium iodide) as well as the variability of different surface markers expression were measured by FACS analysis. LPS- or CpG-matured DCs were eFluor670-labeled and plated at a fixed concentration of 3×10^5 cells/well in a round-bottomed, 96-well plate. BM-MDSCs from WT or *Nos2*$^{-/-}$ mice were used as bulk cells or sorted by FACS into CD11b$^+$Ly6G$^-$Ly6C^{hi} monocytic (M-MDSCs) and CD11b$^+$Ly6G$^+$Ly6C^{lo} granulocytic subsets (G-MDSCs). MDSCs remained resting or activated by 20 μg/mL heat-killed *M. tuberculosis* before they were added at the indicated ratios to the respective cells. Annexin V expression in eFluor670$^+$ cells was measured by FACS after 24 and 48 hours coculture.

Software-based quantification of TUNEL$^+$/CD11c$^+$ cells. Images were processed with the StrataQuest software (TissueGnostics) as described previously (32). Using that software, 3 markers were applied: CD11c, TUNEL, and B220. The B cell area was visualized by B220 for subsequent selection of the T cell area. To achieve optimal cell detection the following parameters were adjusted: (a) CD11c cellular mask and (b) TUNEL shades within the CD11c cellular mask. Scattergrams were created for the evaluation of TUNEL$^+$/CD11c$^+$ cells, allowing the visualization of corresponding positive cells in the source region of interest using the real-time back gating feature. A global measurement algorithm was performed allowing the quantification of CD11c$^+$/TUNEL$^+$ cells within the T cell area of spleen sections. For each section more than 10,000 nucleated cells were assessed, of which more than 100 CD11c$^+$ DCs per T cell area were further analyzed for detection of TUNEL staining.

Statistics. Figures were created and statistics were calculated using the Prism 6 (GraphPad Software) program. Details on the statistical tests used are provided in the figure legends and include 1-way ANOVA with multiple comparisons, 2-way ANOVA, Tukey's post test, and 2-tailed *t* test. *P* values of less than 0.05 were considered significant.

Study approval. All animal experiments were performed according to the national and local animal protection laws as well as after approval and under control of the local authorities (Regierung von Unterfranken, Würzburg, Germany) (no. 55.2-2531.01-64/11 and -2-200).

Author contributions

ER, IE, and UR performed experiments, analyzed the data, and prepared the figures. AB and US contributed research equipment and mice and helped to plan experiments. AB, US, NDP, GW, and MBL arranged the figures and wrote the paper.

Acknowledgments

This publication was funded by the German Research Foundation (DFG) and the University of Wuerzburg in the funding programme Open Access Publishing. This work was supported by the German Research Council (DFG LU851/6-1 and LU851/6-2 to MBL; DFG-CRC 1181, C04 to US). We thank the Major Research Instrumentation TissueFAXS iPLUS analysis station (INST 89/341-1FUGG). We are grateful for the continuous support of Thomas Hünig and Wolfgang Kastenmüller. We also thank Alma Zernecke and Melanie Schott for use of the Cryotome and Nora Müller, Marion Heuer and Vini John for technical assistance or help with experiments.

Address correspondence to: Manfred B. Lutz, Institute of Virology and Immunobiology, University of Würzburg, Versbacherstrasse 7, 97078 Würzburg, Germany. Phone: 49.931.31.81553; Email: m.lutz@vim.uni-wuerzburg.de.

1. Veglia F, Perego M, Gabrilovich D. Myeloid-derived suppressor cells coming of age. *Nat Immunol*. 2018;19(2):108–119.
2. Gabrilovich DI, Ostrand-Rosenberg S, Bronte V. Coordinated regulation of myeloid cells by tumours. *Nat Rev Immunol*. 2012;12(4):253–268.
3. Bronte V, Zanovello P. Regulation of immune responses by L-arginine metabolism. *Nat Rev Immunol*. 2005;5(8):641–654.
4. Mazzoni A, et al. Myeloid suppressor lines inhibit T cell responses by an NO-dependent mechanism. *J Immunol*.

2002;168(2):689–695.
5. Macphail SE, Gibney CA, Brooks BM, Booth CG, Flanagan BF, Coleman JW. Nitric oxide regulation of human peripheral blood mononuclear cells: critical time dependence and selectivity for cytokine versus chemokine expression. *J Immunol*. 2003;171(9):4809–4815.
6. Albina JE, Abate JA, Henry WL. Nitric oxide production is required for murine resident peritoneal macrophages to suppress mitogen-stimulated T cell proliferation. Role of IFN-gamma in the induction of the nitric oxide-synthesizing pathway. *J Immunol*. 1991;147(1):144–148.
7. Wang Z, Jiang J, Li Z, Zhang J, Wang H, Qin Z. A myeloid cell population induced by Freund adjuvant suppresses T-cell-mediated antitumor immunity. *J Immunother*. 2010;33(2):167–177.
8. Dorhoi A, Du Plessis N. Monocytic Myeloid-Derived Suppressor Cells in Chronic Infections. *Front Immunol*. 2017;8:1895.
9. Du Plessis N, et al. Phenotypically resembling myeloid derived suppressor cells are increased in children with HIV and exposed/infected with *Mycobacterium tuberculosis*. *Eur J Immunol*. 2017;47(1):107–118.
10. du Plessis N, et al. Increased frequency of myeloid-derived suppressor cells during active tuberculosis and after recent *mycobacterium tuberculosis* infection suppresses T-cell function. *Am J Respir Crit Care Med*. 2013;188(6):724–732.
11. Knaul JK, et al. Lung-residing myeloid-derived suppressors display dual functionality in murine pulmonary tuberculosis. *Am J Respir Crit Care Med*. 2014;190(9):1053–1066.
12. van Doorn E, Liu H, Huckriede A, Hak E. Safety and tolerability evaluation of the use of Montanide ISA™51 as vaccine adjuvant: A systematic review. *Hum Vaccin Immunother*. 2016;12(1):159–169.
13. Fernández A, Oliver L, Alvarez R, Fernández LE, Lee KP, Mesa C. Adjuvants and myeloid-derived suppressor cells: enemies or allies in therapeutic cancer vaccination. *Hum Vaccin Immunother*. 2014;10(11):3251–3260.
14. Billiau A, Matthys P. Modes of action of Freund's adjuvants in experimental models of autoimmune diseases. *J Leukoc Biol*. 2001;70(6):849–860.
15. Baxter AG. The origin and application of experimental autoimmune encephalomyelitis. *Nat Rev Immunol*. 2007;7(11):904–912.
16. Croxford AL, Kurschus FC, Waisman A. Mouse models for multiple sclerosis: historical facts and future implications. *Biochim Biophys Acta*. 2011;1812(2):177–183.
17. Sadelain MW, Qin HY, Lauzon J, Singh B. Prevention of type I diabetes in NOD mice by adjuvant immunotherapy. *Diabetes*. 1990;39(5):583–589.
18. Armentero MT, Levandis G, Nappi G, Bazzini E, Blandini F. Peripheral inflammation and neuroprotection: systemic pretreatment with complete Freund's adjuvant reduces 6-hydroxydopamine toxicity in a rodent model of Parkinson's disease. *Neurobiol Dis*. 2006;24(3):492–505.
19. Jordan MB, Mills DM, Kappler J, Marrack P, Cambier JC. Promotion of B cell immune responses via an alum-induced myeloid cell population. *Science*. 2004;304(5678):1808–1810.
20. Rössner S, Voigtländer C, Wiethe C, Hänig J, Seifarth C, Lutz MB. Myeloid dendritic cell precursors generated from bone marrow suppress T cell responses via cell contact and nitric oxide production in vitro. *Eur J Immunol*. 2005;35(12):3533–3544.
21. Ribechini E, et al. Novel GM-CSF signals via IFN-γR/IRF-1 and AKT/mTOR license monocytes for suppressor function. *Blood Adv*. 2017;1(14):947–960.
22. Greifenberg V, Ribechini E, Rössner S, Lutz MB. Myeloid-derived suppressor cell activation by combined LPS and IFN-gamma treatment impairs DC development. *Eur J Immunol*. 2009;39(10):2865–2876.
23. Martino A, et al. Mycobacterium bovis bacillus Calmette-Guérin vaccination mobilizes innate myeloid-derived suppressor cells restraining in vivo T cell priming via IL-1R-dependent nitric oxide production. *J Immunol*. 2010;184(4):2038–2047.
24. Lei GS, Zhang C, Lee CH. Myeloid-derived suppressor cells impair alveolar macrophages through PD-1 receptor ligation during Pneumocystis pneumonia. *Infect Immun*. 2015;83(2):572–582.
25. Ostrand-Rosenberg S, Sinha P, Beury DW, Clements VK. Cross-talk between myeloid-derived suppressor cells (MDSC), macrophages, and dendritic cells enhances tumor-induced immune suppression. *Semin Cancer Biol*. 2012;22(4):275–281.
26. Riquelme P, et al. TIGIT. *Nat Commun*. 2018;9(1):2858.
27. Buhles WC, Shifrine M. Increased bone marrow production of granulocytes and mononuclear phagocytes induced by mycobacterial adjuvants: improved recovery of leukopoiesis in mice after cyclophosphamide treatment. *Infect Immun*. 1978;20(1):58–65.
28. Epelman S, Lavine KJ, Randolph GJ. Origin and functions of tissue macrophages. *Immunity*. 2014;41(1):21–35.
29. Swirski FK, et al. Identification of splenic reservoir monocytes and their deployment to inflammatory sites. *Science*. 2009;325(5940):612–616.
30. Montoya M, Edwards MJ, Reid DM, Borrow P. Rapid activation of spleen dendritic cell subsets following lymphocytic choriomeningitis virus infection of mice: analysis of the involvement of type 1 IFN. *J Immunol*. 2005;174(4):1851–1861.
31. Wu AA, Drake V, Huang HS, Chiu S, Zheng L. Reprogramming the tumor microenvironment: tumor-induced immunosuppressive factors paralyze T cells. *Oncoimmunology*. 2015;4(7):e1016700.
32. Schmid M, et al. An Emerging Approach for Parallel Quantification of Intracellular Protozoan Parasites and Host Cell Characterization Using TissueFAXS Cytometry. *PLoS One*. 2015;10(10):e0139866.
33. Kaur S, Kaur H, Singh PP. Induction of colony-stimulating factors by a 30-kDa secretory protein of *Mycobacterium tuberculosis* H37Rv. *Eur Cytokine Netw*. 2004;15(4):327–338.
34. Chen YM, Yang WK, Whang-Peng J, Tsai CM, Perng RP. An analysis of cytokine status in the serum and effusions of patients with tuberculous and lung cancer. *Lung Cancer*. 2001;31(1):25–30.
35. Mitroulis I, et al. Modulation of Myelopoiesis Progenitors Is an Integral Component of Trained Immunity. Cell. 2018;172(1-2):147–161.e12.
36. Arts RJW, et al. Immunometabolic Pathways in BCG-Induced Trained Immunity. *Cell Rep*. 2016;17(10):2562–2571.
37. Kaufmann E, et al. BCG Educates Hematopoietic Stem Cells to Generate Protective Innate Immunity against Tuberculosis. *Cell*. 2018;172(1-2):176–190.e19.
38. Arts RJW, et al. BCG Vaccination Protects against Experimental Viral Infection in Humans through the Induction of Cytokines Associated with Trained Immunity. *Cell Host Microbe*. 2018;23(1):89–100.e5.
39. Rosborough BR, Castellaneta A, Natarajan S, Thomson AW, Turnquist HR. Histone deacetylase inhibition facilitates

GM-CSF-mediated expansion of myeloid-derived suppressor cells in vitro and in vivo. *J Leukoc Biol*. 2012;91(5):701–709.
40. Nicholas D, et al. Quantitative proteomics reveals a role for epigenetic reprogramming during human monocyte differentiation. *Mol Cell Proteomics*. 2015;14(1):15–29.
41. De Smedt T, et al. Regulation of dendritic cell numbers and maturation by lipopolysaccharide in vivo. *J Exp Med*. 1996;184(4):1413–1424.
42. Ato M, Maroof A, Zubairi S, Nakano H, Kakiuchi T, Kaye PM. Loss of dendritic cell migration and impaired resistance to Leishmania donovani infection in mice deficient in CCL19 and CCL21. *J Immunol*. 2006;176(9):5486–5493.
43. Ugel S, et al. Immune tolerance to tumor antigens occurs in a specialized environment of the spleen. *Cell Rep*. 2012;2(3):628–639.
44. Bronte V, Pittet MJ. The spleen in local and systemic regulation of immunity. *Immunity*. 2013;39(5):806–818.
45. Bronte V, et al. Apoptotic death of CD8+ T lymphocytes after immunization: induction of a suppressive population of Mac-1+/Gr-1+ cells. *J Immunol*. 1998;161(10):5313–5320.
46. Bronte V, Serafini P, Mazzoni A, Segal DM, Zanovello P. L-arginine metabolism in myeloid cells controls T-lymphocyte functions. *Trends Immunol*. 2003;24(6):302–306.
47. Goñi O, Alcaide P, Fresno M. Immunosuppression during acute Trypanosoma cruzi infection: involvement of Ly6G (Gr1(+)) CD11b(+)immature myeloid suppressor cells. *Int Immunol*. 2002;14(10):1125–1134.
48. Rodrigues LC, et al. Effect of BCG revaccination on incidence of tuberculosis in school-aged children in Brazil: the BCG-REVAC cluster-randomised trial. *Lancet*. 2005;366(9493):1290–1295.
49. Smaill F, et al. A human type 5 adenovirus-based tuberculosis vaccine induces robust T cell responses in humans despite preexisting anti-adenovirus immunity. *Sci Transl Med*. 2013;5(205):205ra134.
50. Nemes E, et al. Prevention of M. tuberculosis Infection with H4:IC31 Vaccine or BCG Revaccination. *N Engl J Med*. 2018;379(2):138–149.
51. Dietlin TA, Hofman FM, Lund BT, Gilmore W, Stohlman SA, van der Veen RC. Mycobacteria-induced Gr-1+ subsets from distinct myeloid lineages have opposite effects on T cell expansion. *J Leukoc Biol*. 2007;81(5):1205–1212.
52. Lutz MB, et al. An advanced culture method for generating large quantities of highly pure dendritic cells from mouse bone marrow. *J Immunol Methods*. 1999;223(1):77–92.
53. Zal T, Volkmann A, Stockinger B. Mechanisms of tolerance induction in major histocompatibility complex class II-restricted T cells specific for a blood-borne self-antigen. *J Exp Med*. 1994;180(6):2089–2099.
54. Stenger S, Donhauser N, Thüring H, Röllinghoff M, Bogdan C. Reactivation of latent leishmaniasis by inhibition of inducible nitric oxide synthase. *J Exp Med*. 1996;183(4):1501–1514.
55. Green LC, Wagner DA, Glogowski J, Skipper PL, Wishnok JS, Tannenbaum SR. Analysis of nitrate, nitrite, and [15N]nitrate in biological fluids. *Anal Biochem*. 1982;126(1):131–138.